Available online at www.sciencedirect.com
SCIENCE DIRECT®
Journal of Sound and Vibration 273 (2004) 51–75
JOURNAL OF SOUND AND VIBRATION
www.elsevier.com/locate/jsvi

Evaluation of modal density and group velocity by a finite element method

S. Finnveden

MWL, Aeronautical and Vehicle Engineering, KTH, SE-100 44 Stockholm, Sweden

Received 14 October 2002; accepted 15 April 2003

Abstract

A finite element method (FEM), the waveguide-FEM, is used to calculate wave propagation characteristics for built-up thin-walled structures. Such characteristics are determined from a dispersion relation in the form of an eigenvalue problem established from the FE formulation. In particular, vital characteristics such as the modal density, the group velocity and the waveform are evaluated. A description of the evaluation of a dispersion relation for a channel beam, from data given by the FE formulation, is presented. Subsequently, the method for determining the modal density and group velocity from FE input data is shown in detail for the beam structure. To show the versatility of the method a second example considers a statistical energy analysis (SEA), made to establish the degree to which vibrations in a wind tunnel are transmitted to a thin-walled plate mounted into its wall. The critical input datum to the SEA model is the wind tunnel's modal density, which is calculated by the method presented.

1. Introduction

High-frequency vibration analysis benefits from an understanding of the vibrational waves propagating in the structure of interest. Important characteristics of these waves are the wavenumbers, the group velocity and the waveform. Vital characteristics for a statistical energy analysis (SEA) are the modal density and the relation between modal energy and vibration velocity, which depends on the mass distribution and the waveform. For common structural components, such as beams, plates and cylinders, all of these characteristics have been established [1–5]. However, analysis of general structures is often difficult.

The purpose of this paper is to demonstrate how such an analysis may be performed using a computational technique. This technique applies for structures that have arbitrary cross-sectional

E-mail address: svantef@fkt.kth.se (S. Finnveden).

0022-460X/$ - see front matter
doi:10.1016/j.jsv.2003.04.004

properties that are uniform along one direction. For this broad class of structures, it is both adaptable and efficient.

The waveguide finite element method (FEM) uses one- or two-dimensional FE shape functions to describe the motion's x- and y-dependencies, where, without loss of generality it is assumed that the structure is aligned with the z-axis. It follows that the 'nodal' motions are functions of the z-variable. Applying standard FE procedures, a set of coupled wave equations is formulated. For harmonic vibration, the solutions to these wave equations are given by a linear eigenvalue problem, for which efficient numerical algorithms are available.

Possibly, the first application of the waveguide-FE technique was made by Aalami who studied wave propagation in rods with arbitrary cross-section [6]. Studies that are more recent describe wave propagation in laminated composite plates [7], thin-walled beams [8], railway track [9,10], rib-stiffened panels [11], twisted beams [12] anisotropic shells and beams [13,14], fluid-filled pipes [15], a railway car structure [16] and pre-stressed and curved shells [17]. Structures with constant curvature along the waveguide can also be handled [12,17]. The proven versatility of the FEM suggests that the method may apply for any conceivable structure with arbitrary cross-sectional properties that are uniform along one direction.

The following presents, for the first time, methodology for post-processing of waveguide-FE models, useful for vibration analysis and in particular SEA. The presentation is made via two examples.

The first example, in Section 2, considers a U-shaped channel beam with dimensions such that beam theories can apply only in a lower-frequency regime. For this structure, the dispersion relations are solved and the results are compared with those resulting from the Euler and Vlasov beam theories. Upon this basis, the modal density and group velocity for the various wave components are calculated.

The second example, in Section 3, considers a wind tunnel. A major concern for some at the MWL has been to establish the degree to which vibrations in the tunnel are transmitted to a thin-walled plate mounted into its wall. One of the methods for assessing this is based on a simple SEA model in which the critical input datum is the modal density of the wind tunnel. Section 3 presents the waveguide-FE model of the tunnel and the SEA model for estimating the vibration transmission to the plate. A comparison with experimental results is made and discussed.

2. Analysis of vibrational waves in a channel beam

Consider the beam structure shown in Fig. 1. The cross-section element clearly demonstrates the channel beams construction consisting of three plate strips. The principal dimensions are: height, $h = 155$ mm, width, $b = 60$ mm and wall thickness, $t = 4.5$ mm. This steel beam structure was an integral part of a Swedish railway car base frame. Approximate analytical techniques, that are commonly used for such structures, using Euler beam theory or Vlasov beam theory are only accurate in a lower frequency regime.

Adopting a numerical method for the analysis of vibration the geometry or *mesh* used in the waveguide-FEM is depicted in Fig. 2. Note that only the cross-section requires a FE *mesh*. Indeed, the waveguide-FE formulation assumes a polynomial description of the displacements' dependence on the cross-sectional co-ordinates. A linear variation of the in-plane displacements

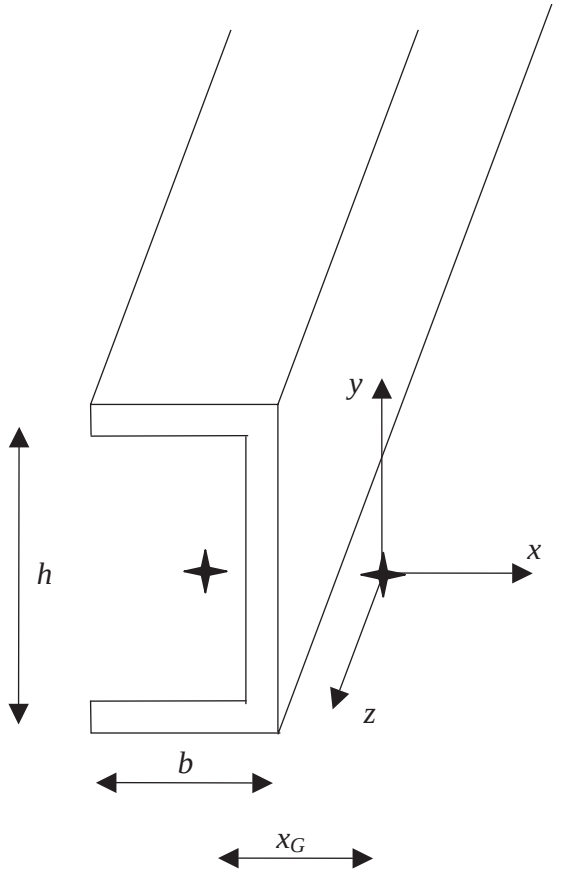

Fig. 1. Sketch of channel beam. The stars indicate the locations of the mass and shear centres.

and a cubic variation of the out-of-plane displacement between the nodes was assumed. A concise description of the waveguide-FEM formulation is detailed in the Appendix.

Application of the waveguide-FEM yields the following homogeneous wave equation for the channel beam

$$\sum_{n=0}^{4} \mathbf{K}_n \frac{\mathrm{d}^n \mathbf{u}}{\mathrm{d}z^n} - \omega^2 \mathbf{M}\mathbf{u} = \mathbf{0}, \tag{1}$$

where ω is the angular frequency, a harmonic time dependence of the form $\mathrm{e}^{-\mathrm{i}\omega t}$ is assumed and suppressed throughout. $\mathbf{K}_n$, $n = 0, \ldots, 4$, are 'stiffness' matrices, $\mathbf{M}$ is the mass matrix and the vector $\mathbf{u}$ contains the 'nodal' displacements as functions of z. Using the element described in the Appendix, these are, for each node, the three displacement components and the rotation about the z-axis. The equations (1) form a set of coupled ordinary differential equations with constant coefficients. The solutions are in the form of exponential functions. Specifically, for a propagating wave, the nodal displacements take the form

$$\mathbf{u}(z) = \mathbf{\Phi}\mathrm{e}^{\mathrm{i}\kappa z}, \tag{2}$$

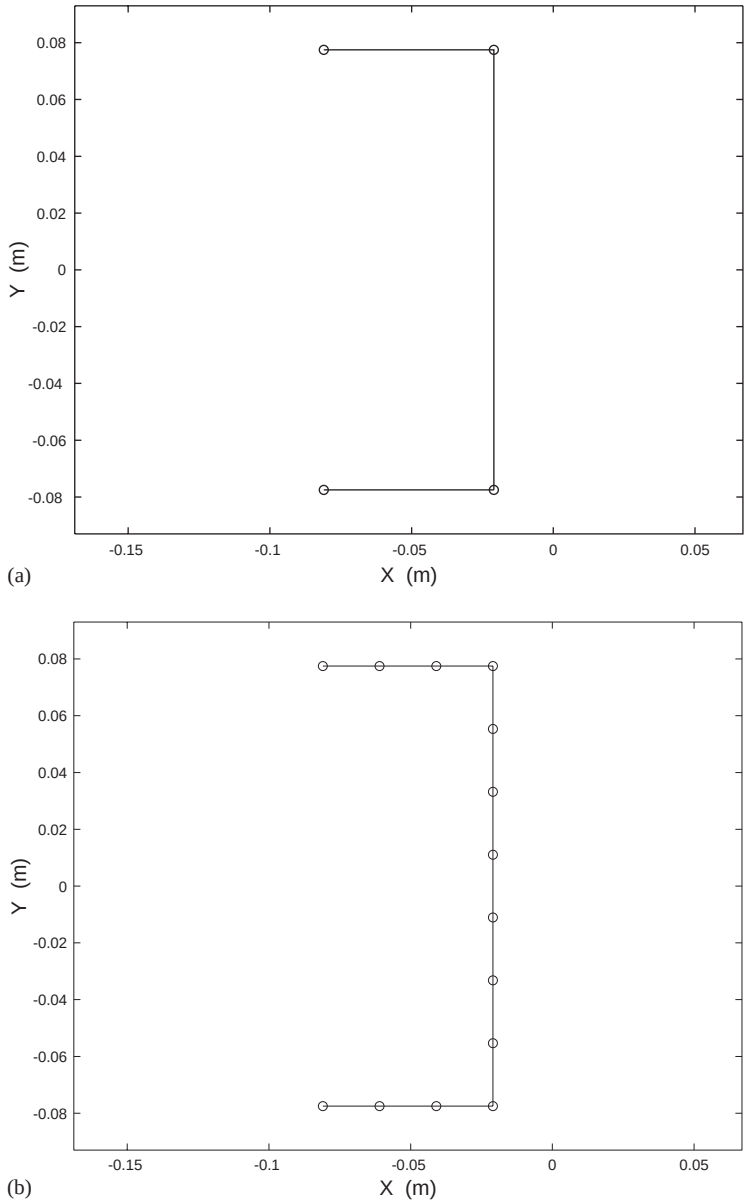

Fig. 2. (a) Simple waveguide-FE model of channel beam. Circles indicate node positions. (b) As (a) but detailed waveguide-FE model.

where the vector $\mathbf{\Phi}$ defines the waveform and κ is the wavenumber. Now, Eq. (2) is inserted into Eq. (1), upon which a two-parameter (κ, ω) eigenvalue problem follows

$$[\mathbf{K}(\kappa) - \omega^2 \mathbf{M}]\mathbf{\Phi} = \mathbf{0}, \tag{3}$$

where

$$\mathbf{K}(\kappa) = \sum_{n=0}^{4} (\mathrm{i}\kappa)^n \mathbf{K}_n. \tag{4}$$

Eq. (3) can either, for a given frequency, ω, be solved as a polynomial eigenvalue problem in κ or, for a given wavenumber, κ, as a linear generalised eigenvalue problem in ω. Section 2.2 presents the wave solutions resulting from these procedures and from the applications of beam theories. First, some important properties of the matrices in Eq. (3) and the procedures used to solve the eigenvalue problems are discussed.

2.1. Properties of the matrices and solution procedure

The matrices defined above have some properties that will be stated in the following.

These properties apply for structures built up by the waveguide-FE detailed in the Appendix. It is important to note that only conservative motion is considered, unless explicitly stated otherwise, and therefore all the matrices $\mathbf{K}_n$, $n = 0, \ldots, 4$, and $\mathbf{M}$ are real. Also, the mass matrix $\mathbf{M}$ is symmetric and positive definite. For the thin-walled element used, the matrix $\mathbf{K}_3$ is zero. The matrices $\mathbf{K}_4$, $\mathbf{K}_2$ and $\mathbf{K}_0$ are symmetric and $\mathbf{K}_1$ is anti-symmetric. It follows that $\mathbf{K}$, defined by Eq. (4), is Hermitian for real-valued κ. Consequently, the eigenfrequencies are real valued for propagating undamped waves (real κ).

The left eigenvector $\mathbf{\Phi}^{(L)}$ is defined by

$$\mathbf{\Phi}^{(L)\mathrm{T}}[\mathbf{K}(\kappa) - \omega^2\mathbf{M}] = \mathbf{0}. \tag{5}$$

The left eigenvector equals the complex conjugate of the right eigenvector, given by Eq. (3),

$$\mathbf{\Phi}^{(L)} = \mathbf{\Phi}^*, \tag{6}$$

since $\mathbf{K}$ is Hermitian and $\mathbf{M}$ is real and symmetric.

For an eigenvalue analysis the mass matrix $\mathbf{M}$ is Cholesky factorised so that $\mathbf{M} = \mathbf{m}^{\mathrm{T}}\mathbf{m}$, where $\mathbf{m}^{\mathrm{T}}$ denotes transpose of a Cholesky matrix. Eq. (3) is transformed into a standard linear eigenvalue problem [18, p. 442]

$$[\mathbf{A} - \omega^2\mathbf{I}]\mathbf{x} = \mathbf{0}, \tag{7}$$

where

$$\mathbf{A}(\kappa) = (\mathbf{m}^{\mathrm{T}})^{-1}\mathbf{K}(\kappa)\mathbf{m}^{-1};\ \ \mathbf{m}^{\mathrm{T}}\mathbf{m} = \mathbf{M}; \mathbf{\Phi} = \mathbf{m}^{-1}\mathbf{x}. \tag{8}$$

This standard procedure increases numerical efficiency and stability. It is applied in the following but is not discussed further.

As stated earlier, the eigenvalue problem (3) is solved for a given wavenumber κ in form (7), but if instead, Eq. (3) is considered for a given frequency, ω, it defines a polynomial eigenvalue problem for the wavenumbers. This polynomial eigenvalue problem is as in Ref. [11, Appendix A] transformed to a generalised linear eigenvalue problem, which can be solved by standard methods.

Tisseur and Meerbergen report that polynomial eigenvalue problems, which are linearised, can be numerically ill-conditioned [19]. Such problems might be an issue for the waveguide-FEM but

have not yet been encountered. Possibly, the linearisation procedure proposed in Ref. [11] has a stabilising effect, since it eliminates redundant variables. Nevertheless, Eq. (7) is the preferred formulation for determining propagating waves, since it gives a stable numerical problem and evaluates roughly 100 times quicker than the linearised polynomial eigenvalue formulation.

2.2. Wave solutions

This section describes the waves that propagate in the channel beam. The solutions derived from approximate analytical beam theories are compared to the numerical solution provided by the waveguide-FEM and the regions of validity for the different methods are discussed.

2.2.1. Euler beam

For an Euler beam, the wavenumbers of the propagating waves with transverse motion in the x and y directions, longitudinal motion and rotational motion are given by

$$k_{bx} = \sqrt{\omega\sqrt{\rho A/EI_y}}, \quad k_{by} = \sqrt{\omega\sqrt{\rho A/EI_x}},$$
$$k_l = \omega/\sqrt{E/\rho}, \quad k_r = \omega\sqrt{\rho I_r/GI_t}, \tag{9}$$

where ρ is the density, E is Young's modulus, A is the cross-sectional area, I_x and I_y are the area moments about the x- and y-axis calculated for the section centre, $I_r = I_x + I_y$ and GI_t is the Saint–Venant rotational rigidity [20, p. 45]. The waveguide-FE is based on thin shell theory and hence for reason of comparison, the transverse and rotational wavenumbers in Eq. (9) are evaluated with a Young's modulus $E' = E/(1-\nu^2)$, where ν is the Poisson ratio.

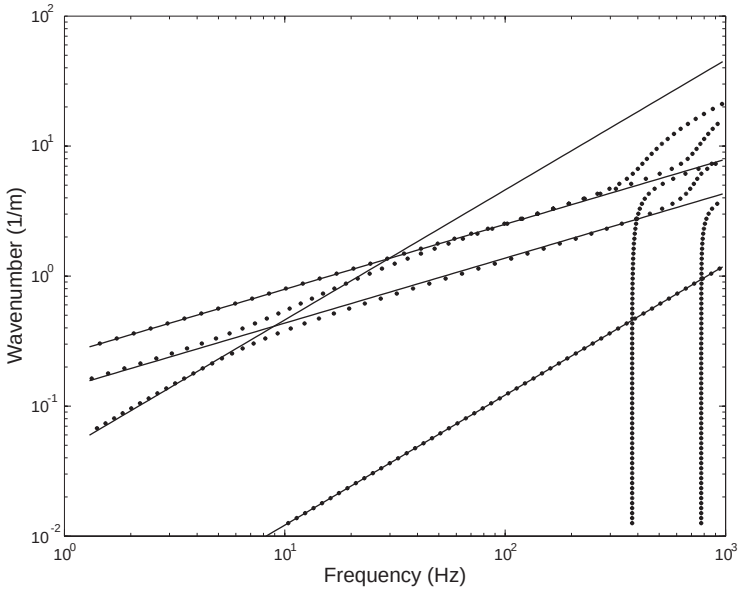

Fig. 3. Wavenumbers. Dots, simple waveguide-FE model; solid line, Euler beam theory, Eq. (9). In the low-frequency end, these are from top to bottom: k_{bx}, k_{by}, k_r and k_l.

Fig. 3 compares the wavenumbers described by Eqs. (9) with those calculated by the simple waveguide-FE model in Fig. 2a. At lower frequencies, the models agree except for a minor difference in the rotational wave. However, already at 5 Hz the rotational wavenumbers differ largely and in a cross-over region so the wavenumbers for transverse motion in the y direction. Consequently, simple beam theory does not provide an accurate description of all the waves in the beam, except for very low frequencies, and a more elaborate theory is required.

2.2.2. Vlasov beam

The Euler beam theory does not include the warping resistance, which for an open cross-section significantly impedes the rotational motion [20]. Moreover, for structures having different shear and mass centres, there are inertia couplings of the flexural waves and the rotational wave. The Vlasov beam theory attributes these two effects, resulting in the following set of coupled differential equations, which are taken here from Friberg [21] for the case of equal y co-ordinate for the mass and shear centres

$$\begin{aligned} &EI_y u'''' + \rho\omega^2 I_y u'' - \rho A\omega^2 u = 0,\\ &EI_x v'''' + \rho\omega^2 I_x v'' - \rho A\omega^2 (v + x_G\phi) = 0,\\ &EI_\omega \phi'''' + (\rho I_\omega \omega^2 - GI_t)\phi'' - \rho\omega^2 (I_r + x_G^2 A)\phi - \rho A\omega^2 x_G v = 0,\\ &-EAw'' - \rho A\omega^2 w = 0. \end{aligned} \tag{10}$$

Above, u, v and w are the displacements at the shear centre in the x, y and z directions, respectively, ϕ denotes the rotation about the z-axis and prime denotes differentiation with respect to the z variable. EI_ω is the warping rigidity and x_G is the distance between the shear centre and the mass centre [20, p. 202]. Shear deformation is not considered in the Vlasov theory (10). Friberg followed Vlasov who included the rotary and warping inertia terms. Normally, these inertia effects are small compared to the effects of shear deformation, but have been retained for completeness.

Fig. 4 compares the wavenumbers derived from the set of equations (10) with those calculated by the simple waveguide-FE model. As can be seen, the agreement is excellent up to the frequencies where the shear waves propagate. The simple FE model predicts the cut-on frequencies for these waves at 377 and 776 Hz, respectively.

Fig. 5 shows the wavenumbers calculated by the detailed FE model. It predicts cut-on frequencies for the two shear waves at the slightly lower frequencies of 373 and 772 Hz. For reference, Fig. 5 also shows the free flexural wavenumber for a plate with a wall-thickness $t =$ 4.5 mm, which is given by [1]

$$k_p = \sqrt{\omega}\left[\frac{\rho t}{Et^3/12(1-\nu^2)}\right]^{1/4}. \tag{11}$$

Fig. 6 shows, as an example, the waveform for the four waves that propagate at 20 Hz. Similarly, Fig. 7 shows two complex waveforms at approximately 2 kHz.

The shear waves may have been predicted with Vlasov–Timoshenko beam theory. This theory, however, is complicated and it is difficult to find the cross-sectional parameters for such a model, especially so for more complex cross-sections. Indeed, the determination of these parameters is still subject to research, e.g. [22]. In contrast to this, the waveguide-FE model requires only the

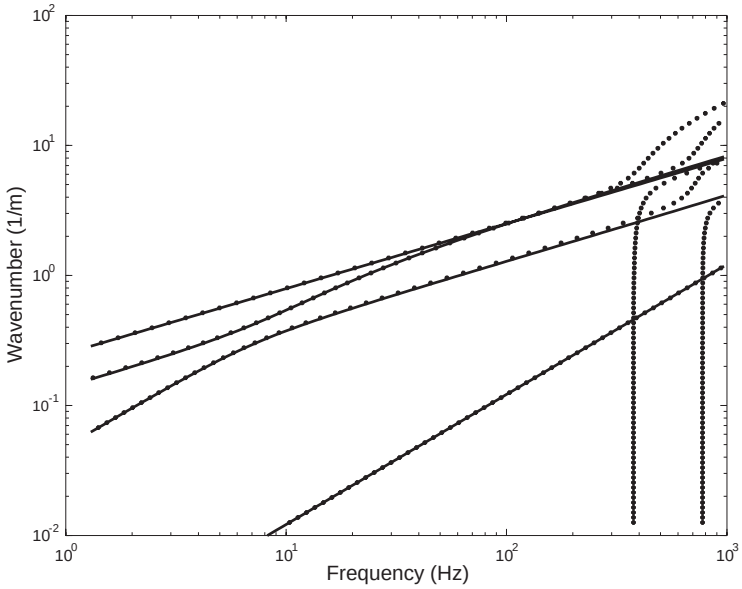

Fig. 4. Wavenumbers. Solid line, Vlasov beam theory, Eq. (10); dots, simple waveguide-FE model.

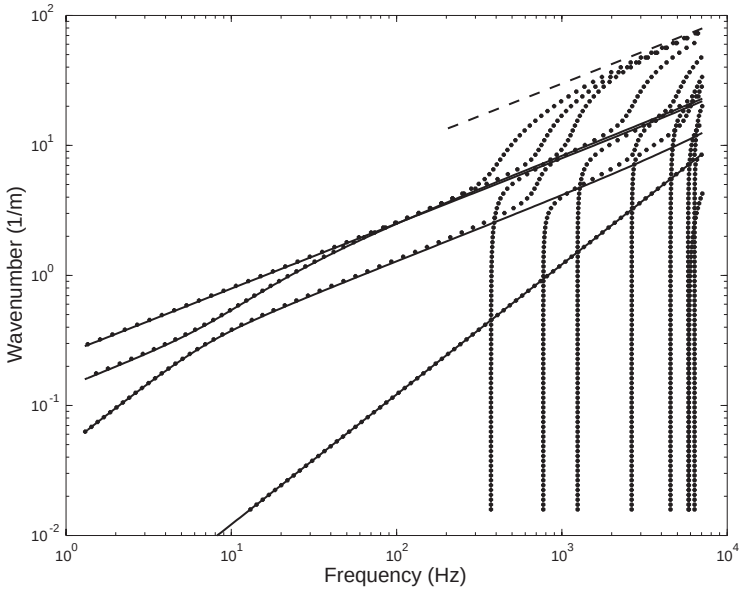

Fig. 5. Wavenumbers. Solid line, Vlasov beam theory; dashed line, plate theory, Eq. (11); dots, detailed waveguide-FE model.

nodal co-ordinates and, for each element, Young's modulus, the Poisson ratio, the density and the wall thickness. This technique should therefore be useful in engineering practice where it is valuable to know the vibrational wavelengths and waveforms. Moreover, the number of

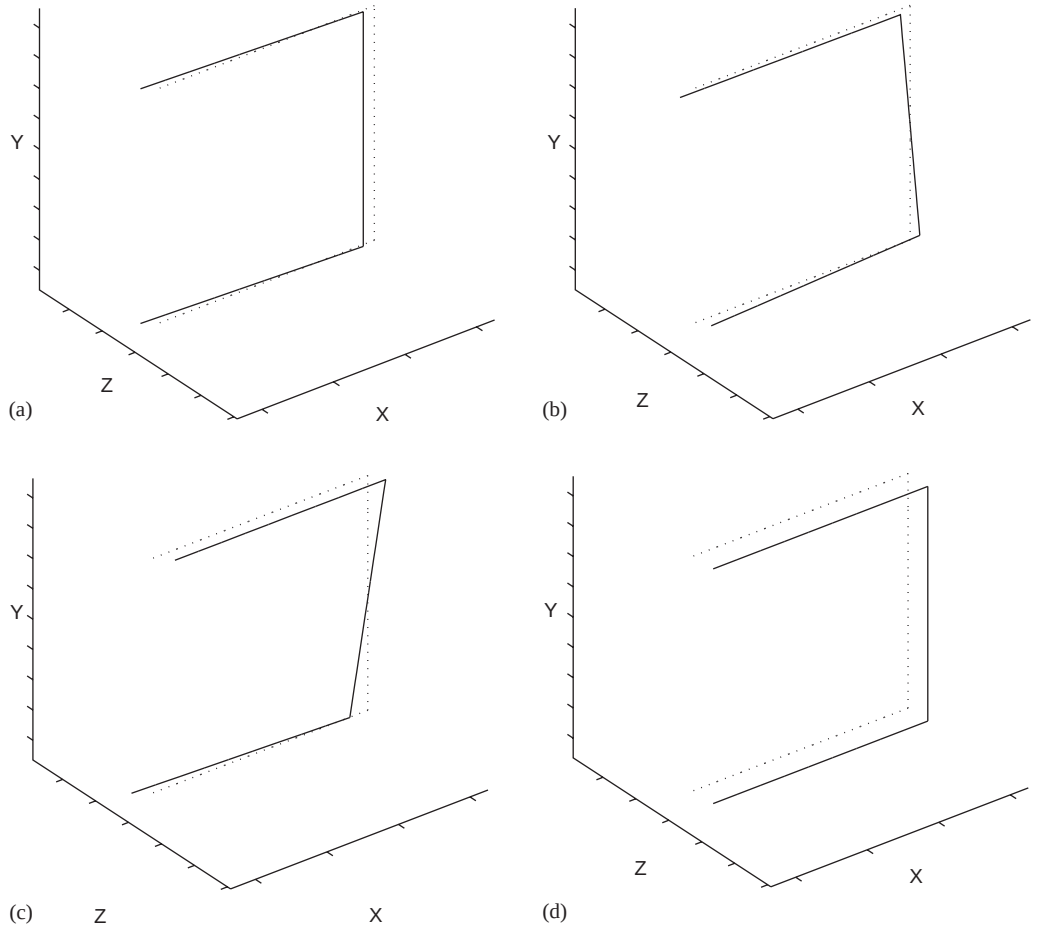

Fig. 6. (a) Waveform at $f = 20$ Hz, $\kappa = 1.12$ m^{-1}. (b) Waveform at $f = 20$ Hz, $\kappa = 0.96$ m^{-1}. (c) Waveform at $f = 20$ Hz, $\kappa = 0.57$ m^{-1}. (d) Waveform at $f = 20$ Hz, $\kappa = 0.024$ m^{-1}.

resonances and the speed by which the vibrational energy propagates in the structure can be determined, as will be explained in the following.

2.3. Modal density and group velocity

In Section 2.1 it was shown that the matrices $\mathbf{K}_n$ and $\mathbf{M}$ are real-valued for structures without damping and $\mathbf{K}$ is Hermitian whereas $\mathbf{M}$ is symmetric. Thus, if $\kappa = \kappa(\omega)$ is a real eigenvalue to Eq. (3) and $\mathbf{\Phi}$ is the corresponding eigenvector, then $-\kappa$ is also an eigenvalue with eigenvector $\mathbf{\Phi}^*$. One of the solutions to the equations of motion (1) is therefore given by

$$\mathbf{U} = a(\mathbf{\Phi}e^{i\kappa z} + \mathbf{\Phi}^* e^{-i\kappa z}) = b(\mathrm{Re}(\mathbf{\Phi})\cos(\kappa z) + i\,\mathrm{Im}(\mathbf{\Phi})\sin(\kappa z)), \tag{12}$$

where a and b are constants, possibly complex.

To satisfy general boundary conditions for a finite length waveguide, all solutions to Eq. (1) are required, including all the evanescent near-field solutions. One particular boundary condition,

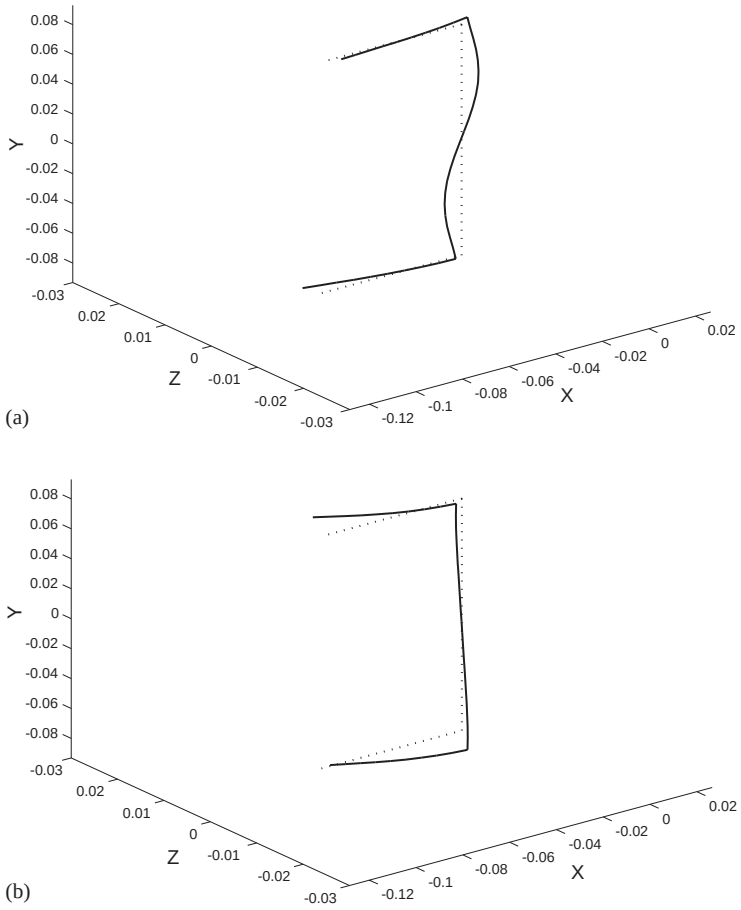

Fig. 7. (a) Waveform at $f = 1985$ Hz, $\kappa = 13.04$ m^{-1}. (b) Waveform at $f = 1970$ Hz, $\kappa = 6.55$ m^{-1}.

however, is fulfilled for the propagating wave solutions, without any interaction between them. For structures built-up by the element detailed in the Appendix, this is the 'shear diaphragm' condition, for which the motion in the x–y plane is blocked and the motion in the z direction is free. It follows that the eigenmodes of a waveguide of length L, obeying this 'convenient' boundary condition, are of form (12), when κ is given by

$$\kappa = p\pi/L, \tag{13}$$

where p is a positive integer. Hence, the eigenfrequencies, $\omega_{p.r}$ are given by the standard eigenvalue problem that follows from Eq. (3) where κ takes the values given by Eq. (13). The eigenvectors $\mathbf{\Phi}_{p.r}$ and the trigonometric functions in (12) specify the corresponding eigenmodes $\mathbf{\Psi}_{p.r}$.

For waveguides that are many wavelengths long, the modal density is asymptotically independent of the boundary condition at the ends. Hence, it follows from the discussion previous to Eq. (13) that the asymptotic modal density, for branch r of the dispersion relations, is

given by

$$n_r(\omega) = \frac{\partial N_r}{\partial \omega} \approx \frac{\partial(\kappa_r L/\pi)}{\partial \omega} = \frac{L}{\pi}\frac{\partial \kappa_r}{\partial \omega}. \tag{14}$$

where $N_r(\omega)$ is the mode count for branch r, i.e., the number of resonances below frequency ω. If the wavenumbers $\kappa_r = \kappa_r(\omega)$ have continuous derivatives, the modal density may alternatively be given by

$$n_r(\omega) = \frac{L}{\pi c_{g.r}}, \quad c_{g.r} = \frac{\partial \omega}{\partial \kappa_r}, \tag{15}$$

where $c_{g.r}$ is the group velocity for the considered wave type, i.e., the speed by which wave energy propagates along the waveguide.

2.3.1. Evaluation of the group velocity

The modal density $n_r(\omega)$ and the group velocity $c_{g.r}(\omega)$ may be calculated by numerical differentiation based on the values of wavenumbers at two adjacent frequencies or from the difference of frequencies at two adjacent wavenumbers. This requires that the solutions to the dispersion relations be categorised, so that the different branches can be identified. In light of the complexity of dispersion curves, such as Fig. 5, this is not straightforward when one branch approaches another. Some linear algebra illustrates an immediate remedy. First, evaluate the derivative of Eq. (3) with respect to wavenumber

$$\frac{\partial}{\partial \kappa}([\mathbf{K}(\mathrm{i}\kappa) - \omega^2\mathbf{M}]\mathbf{\Phi}) = \left[\frac{\partial \mathbf{K}(\mathrm{i}\kappa)}{\partial \kappa} - 2\omega\frac{\partial \omega}{\partial \kappa}\mathbf{M}\right]\mathbf{\Phi} + [\mathbf{K}(\mathrm{i}\kappa) - \omega^2\mathbf{M}]\frac{\partial \mathbf{\Phi}}{\partial \kappa} = \mathbf{0}. \tag{16}$$

Multiply this equation from the left by the left-eigenvector, $\mathbf{\Phi}^{(L)^{\mathrm{T}}} = \mathbf{\Phi}^{\mathrm{H}}$. Then, by virtue of Eq. (5), one has

$$\mathbf{\Phi}^{\mathrm{H}}\left[\frac{\partial \mathbf{K}}{\partial \kappa} - 2\omega\frac{\partial \omega}{\partial \kappa}\mathbf{M}\right]\mathbf{\Phi} = \mathbf{0}. \tag{17}$$

This is, since $\partial\omega/\partial\kappa$ is a scalar, equally written as

$$c_{g.r} = \frac{\partial \omega}{\partial \kappa_r} = \frac{\mathbf{\Phi}^{\mathrm{H}}\mathbf{K}'\mathbf{\Phi}}{2\omega\mathbf{\Phi}^{\mathrm{H}}\mathbf{M}\mathbf{\Phi}}, \tag{18}$$

where

$$\mathbf{K}' = \frac{\partial \mathbf{K}(\mathrm{i}\kappa_r)}{\partial \kappa_r} = \sum_{n=1}^{4} n\mathrm{i}^n\kappa_r^{n-1}\mathbf{K}_n. \tag{19}$$

Eq. (18) can be evaluated considering one solution of the dispersion relations only. It is on a general form and may be applied to any structure built up by a combination of the waveguide-FEs presented in Refs. [6–17]. It is considered to be the most important result of the present work.

Fig. 8 compares the group velocities calculated by Eq. (18) with those resulting from the simple beam theory (9). The group velocities calculated for the non-dispersive longitudinal wave agree at all frequencies. The velocities for the flexural wave with transverse motion in the x direction agree

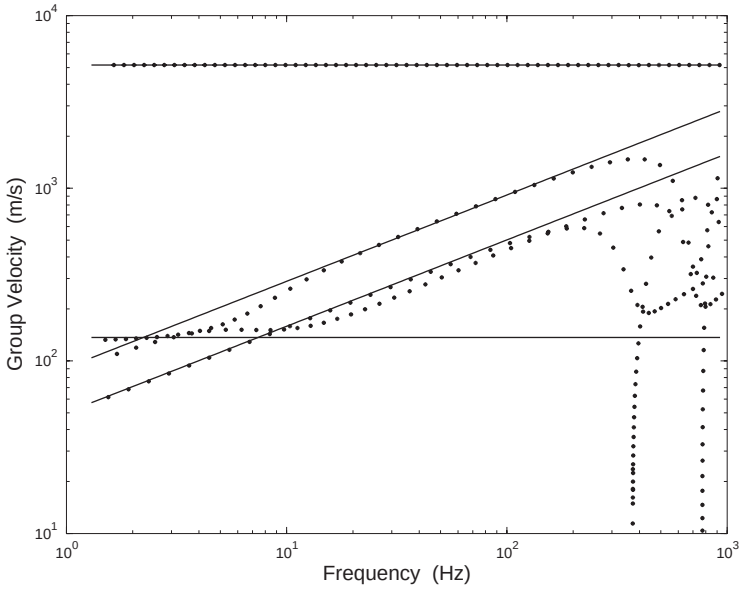

Fig. 8. Group velocity for waves in channel beam. Solid lines, simple beam theory, calculated from Eq. (9); dots, Eq. (19) based on detailed waveguide-FE model.

up until the cross-sectional shear becomes important at approximately 200 Hz. In the cross-over regime, 2–20 Hz, the flexural wave with transverse motion in the y direction and the rotational wave are strongly coupled and the Euler theory does not describe the wave motion. Above this regime, the group velocities agree for the flexural wave up until 200 Hz. The group velocity for the rotational wave, however, is not predicted by simple beam theory.

The group velocity is an important characteristic of a wave. It plays a critical role as input datum for a wave intensity analysis (WIA) [23] and for wave approach calculation of coupling loss factors in a SEA, e.g., [2,3,24]. It turns out that Eq. (18) is useful for such energy analyses.

2.3.2. *Evaluation of the total modal density in frequency bands*

In certain circumstances, a SEA will describe all the wave types in a substructure by one SEA element, an example is given in Section 3. In such a situation, the modal density in a frequency band between frequencies ω_l and ω_u is given by

$$n = \frac{N_{tot}(\omega_u) - N_{tot}(\omega_l)}{\omega_u - \omega_l}, \tag{20}$$

where from Eq. (13), the asymptotic mode count N_{tot} for a waveguide of length L is given by

$$N_{tot}(\omega) = \sum_r \kappa_r(\omega) L/\pi. \tag{21}$$

κ_r is a real-valued eigenvalue to the algebraic eigenvalue problem (3) for a given frequency ω.

Fig. 9 shows for the channel beam in Fig. 1, with length $L = 1$ m, the total mode count and the normalised modal density evaluated for narrow bands (2.8% bandwidth) and third-octave bands. As expected the mode count increases considerably at the cut-on frequency for the first shear

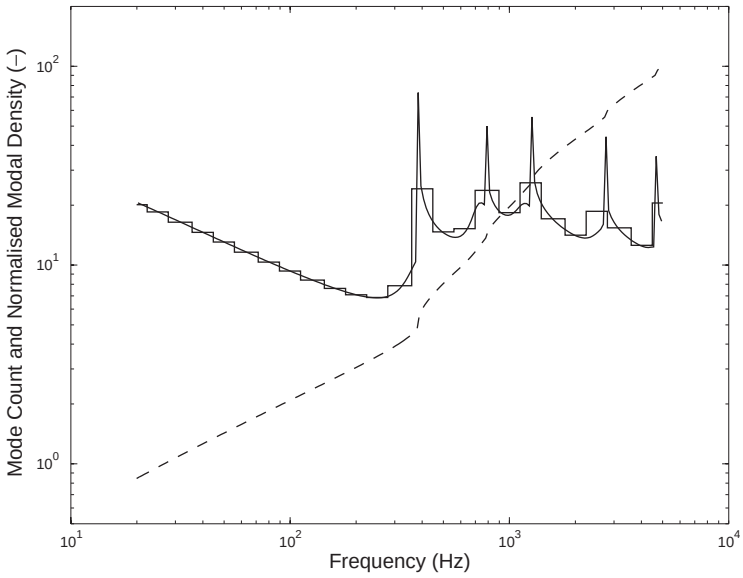

Fig. 9. Dashed line, total asymptotic mode count for a 1 m long channel beam, Eq. (21); solid lines, normalised modal density, $n_{norm} = n\sqrt{E/\rho}/L$, in 2.8% narrow bands and third-octave bands.

wave. Also at higher cut-on frequencies notches appear in the curve indicating a high modal density.

2.3.3. *Modal density for individual branches*

Different wave types have different group velocities and often each wave transmits different amounts of energy at junctions between structural elements. An SEA of, e.g., a beam or a plate structure therefore models transverse and in-plane waves with separate SEA elements. Similarly, an SEA of the channel beam may consider the different wave types as separate elements.

The modal density can be evaluated for discrete frequencies from Eqs. (15) and (18). It appears that the modal density is infinite at the cut-on frequencies. However, within any frequency band, which includes a singularity the modal density must be integrable since the number of resonances in a frequency band is finite for a finite length structure.

For lower frequencies, it is possible to identify the branches of the dispersion curve in Fig. 5. The modal density for branch r is then given by

$$n_r = \frac{L}{\pi}\frac{\kappa_r(\omega_u) - \kappa_r(\omega_l)}{\omega_u - \omega_l}. \tag{22}$$

At higher frequencies, the identification of branches is intricate and an automatic procedure is needed. Bocquillet et al. [25] suggested one such procedure which is applied here in a slightly modified form.

The eigenvectors $\mathbf{x}(\kappa)$ resulting from Eq. (7) are orthonormal:

$$\mathbf{x}_p^{\mathrm{T}} * \mathbf{x}_r = \delta_{pr}, \tag{23}$$

where δ_{pr} the Kronecker delta. Now, if the wavenumber is slightly increased to $\kappa + \Delta\kappa$, it is expected that all the eigenvectors $\mathbf{x}(\kappa + \Delta\kappa)$ are almost orthogonal to $\mathbf{x}_r(\kappa)$, except for the one that

belongs to branch r. Thus, it is possible to categorise the eigenvectors and, consequently, to define the individual dispersion curves of the form $\omega = \Omega_r(\kappa)$. Linear interpolation then determines the wavenumbers $\kappa_r(\omega_u)$ and $\kappa_r(\omega_l)$, upon which expression (22) for the modal density can be evaluated.

This procedure breaks down whenever two branches cross; e.g., in Fig. 5, the dispersion curve for the longitudinal wave crosses the one for the first shear wave at approximately 380 Hz. At this frequency, the two eigenvectors will be nearly orthogonal, yet arbitrary linear combinations of the waveforms for the longitudinal wave and the shear wave. To handle this, the solution to the dispersion relations at several wavenumbers needs to be considered when sorting the branches. This, however, is beyond the scope of the present article.

To conclude this section, the procedures for devising wave equations for a channel beam using FE procedures have been recapitulated. Upon this basis, a technique for post processing the solutions to the wave equations producing the modal density and group velocity was demonstrated. The most important result being Eq. (18). In the following section, the technique will be applied to a real-life structure: a wind tunnel.

3. Structure-borne sound transmission in a wind tunnel

The Marcus Wallenberg Laboratory houses a high-speed, low-noise acoustic flow duct that allows for flow velocities up to 130 m/s and has a background noise level less than 25 dB(A). It has been extensively used for studies of acoustic transmission in ventilation and exhaust systems and for investigations of turbulent boundary layer (TBL) excitation of vibrations in shell structures [26].

For the TBL investigations, an aperture was made in the wind tunnel wall where a thin-walled aluminium plate was mounted. Its TBL-induced vibrations and the radiated sound power was measured. A sketch of the tunnel cross-section where the plate is mounted is shown in Fig. 10. The length of the test plate was 768 mm.

The TBL wall pressure, of course, induces vibrations in both the aluminium plate and the tunnel. A critical question then is, whether the measured plate vibrations are predominantly

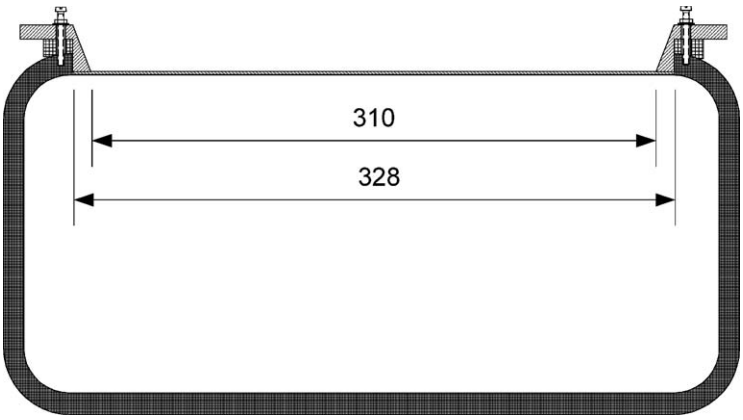

Fig. 10. Cross-section of wind tunnel where a thin-walled plate is mounted. Units are in mm.

directly induced by the TBL or if a substantial contribution is indirectly given by the structure-borne sound transmission of vibrations from the tunnel. To aid the assessment of this, a simple SEA model was made. The critical input datum to the SEA model is the tunnel's modal density, which is calculated with the procedures developed in the previous section. This investigation is explained in the following.

3.1. Sea model

At higher frequencies, SEA should provide, at least, the correct order of magnitude of vibration energies and coupling powers. A simple SEA model considers the flexural vibrations of the test plate as one SEA element and the tunnel as another. The vibration energies are given by [2]

$$\begin{bmatrix} M_1 + C & -C \\ -C & M_2 + C \end{bmatrix} \begin{bmatrix} E_{m.1} \\ E_{m.2} \end{bmatrix} = \begin{bmatrix} P_{in.1} \\ P_{in.2} \end{bmatrix}, \tag{24}$$

where subscript 1 refers to the test plate and subscript 2 to the tunnel. $P_{in.i}$ is the injected power into subsystem i, M_i is the modal overlap, C is the conductivity and $E_{m.i}$ the modal energy (vibration energy per mode times analysis bandwidth). The conductivity is defined through the ansatz (24), whereas one has

$$E_{m.i} = E_i/n_i, \quad M_i = \eta_i \omega n_i, \tag{25}$$

where η_i is the loss factor of element i, n_i is the modal density and E_i is the time-averaged vibration energy in the considered frequency band.

The conductivity and the modal overlap factors are positive and thus the SEA equation is a potential flow model where energy flows from high temperature (modal energy) to low temperature. Consequently, if power is injected into the tunnel only, Eq. (24) indicates that the test plate vibration is restricted by

$$E_{m.1} \leqslant E_{m.2}. \tag{26}$$

For reverberant vibrations, the kinetic and strain energies are on average equal and it follows that

$$\frac{\rho_1 T_{p.1}}{n_1/A_1} \langle v_1^2 \rangle \leqslant \frac{\rho_2 (2h + 2b) T_{p.2}}{n_2/L_2} \langle v_2^2 \rangle, \tag{27}$$

where h, b and L_2 are the tunnel height, width and length, $T_{p.i}$ is the wall thickness, ρ_i is the density, A_1 is the plate area and $\langle v_i^2 \rangle$ is the mean square spatial averaged vibration velocity.

The aperture alters the tunnel's wave pattern considerably and the calculation of the conductivity would not be straightforward. Also, the modal overlap factors need be determined before the application of Eq. (24). The application of Eq. (27) is much simpler, only the total mass and modal density are required and for the large tunnel structure, these are not much affected by the aperture.

3.1.1. Test plate modal density

The test plate is a thin-walled aluminium plate having its first resonance at approximately 90 Hz. Below this frequency the SEA model (24) is useless. At somewhat higher frequencies, the

plate's modal density is estimated by the asymptotic expression [1]

$$n = \frac{A}{3.6 c_L T_p}, \quad c_L = \sqrt{\frac{E/(1-\nu^2)}{\rho}}. \tag{28}$$

3.1.2. Tunnel modal density

The tunnel is a steel structure that supports many different wave types. At lower frequencies it acts like a beam and at higher frequencies it could be likened to a plate assembly. In the high-frequency region, the tunnel modal density, neglecting the in-plane waves, can thus be estimated from Eq. (28). It follows from Eq. (27) that the velocity level difference between the plate and the tunnel is restricted by

$$\Delta L_v = 10 \log_{10}\left(\frac{\langle v_1^2 \rangle}{\langle v_2^2 \rangle}\right) \leqslant 10 \log_{10}\left(\frac{\rho_2 c_{L2} T_{p.2}^2}{\rho_1 c_{L1} T_{p.1}^2}\right) \approx 22 \text{ dB}. \tag{29}$$

Thus, in the high-frequency region, the frequency and space-averaged plate vibration level will, regardless of coupling strength and levels of damping, not exceed that for the tunnel by more than 22 dB when the tunnel only is excited.

Now, to find the limits for the 'low' and 'high' frequency regions and to study the intermediate region, a waveguide-FE model of the wind tunnel was made, based on the FE mesh in Fig. 11. The calculated wavenumbers are shown in Fig. 12 as are the flexural wavenumbers for a 12 mm steel plate and the wavenumbers calculated for a Timoshenko beam, supporting two transverse, one axial and one torsional waves plus, at higher frequencies, two shear waves. The Timoshenko theory predicts the wavenumbers accurately up to approximately 100 Hz, except for a minor deviation for the rotational wave, possibly caused by the use of Saint–Venant's torsion theory,

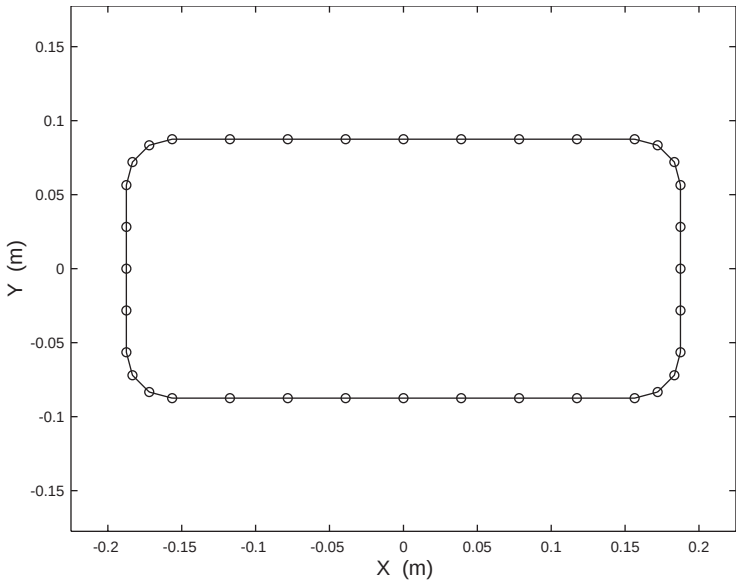

Fig. 11. Waveguide-FE model for wind tunnel. Circles indicate node locations.

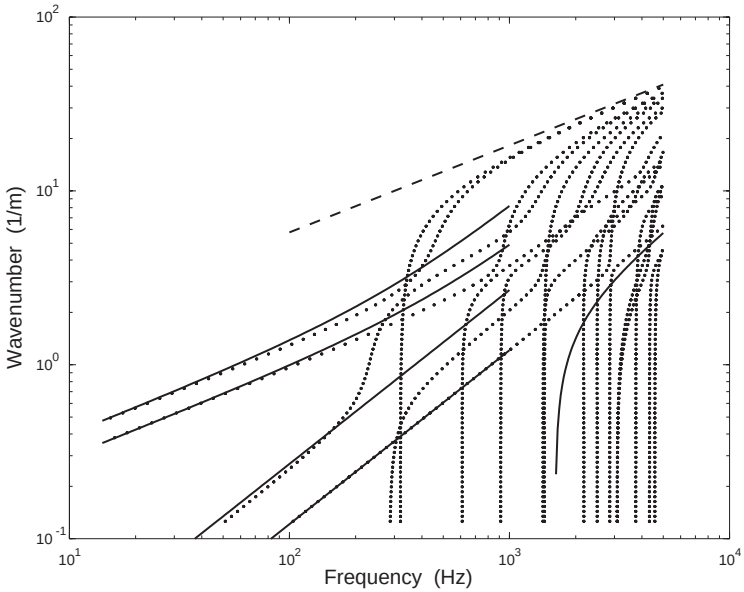

Fig. 12. Dispersion relations for wind tunnel. Solid lines, Timoshenko beam theory; dashed line, thin-walled plate; dots, waveguide-FE results.

neglecting the warping restraint [20]. Fig. 13 shows the waveforms for the first two higher order cross-sectional waves having cut-off frequencies around 300 Hz.

The results in Fig. 12 are the basis for the evaluation of the tunnel's modal density as described in Section 2. Eq. (27) then gives an upper limit for the transmission of vibration from the tunnel to the plate. Fig. 14 shows this conservative SEA estimate of the plate vibration, normalised with the tunnel vibration, for three different values of the tunnel's modal density based on: Timoshenko beam theory, plate theory and the waveguide-FE model. As can be seen, the value based on the waveguide-FE model agrees with the beam theory below 125 Hz and, to a somewhat lesser degree, with the plate theory above 300 Hz; thus defining the low- and high-frequency regions discussed above.

Fig. 14 also shows the velocity level difference measured when a shaker excited the tunnel. This measurement is not fully representative for the case when there is flow within the wind tunnel, since the TBL excites the tunnel differently. Moreover, with flow there is a large static pressure on the structure, which significantly changes the frequencies and mode shapes of both the tunnel and the plate. Nevertheless, the measurement provides one estimate of the structure-borne sound contribution to the plate vibrations and it confirms that the alternative SEA estimate (27), which applies equally for shaker excitation and TBL excitation, is indeed conservative.

In conclusion, the Waveguide-FE-based SEA estimate in Fig. 14 gives a conservative estimate of the maximum contribution to the test plate vibration caused by the tunnel vibration. Thus, if under operation the measured ratio of test plate vibrations to the tunnel vibrations is much larger than the ratio displayed in Fig. 14, one can safely conclude that the test plate vibrations are induced by the TBL only.

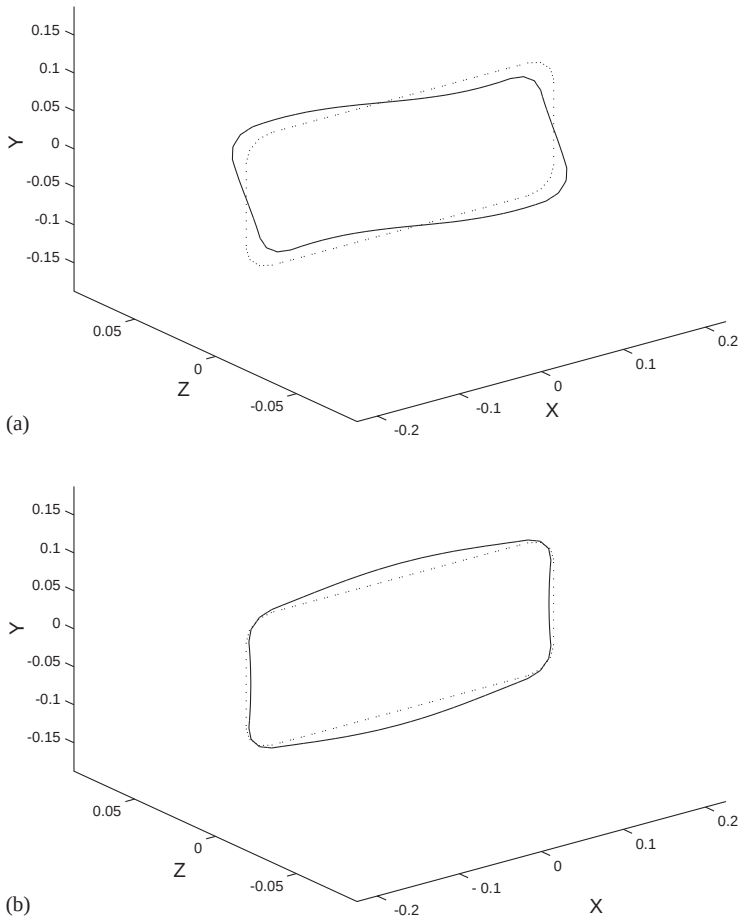

Fig. 13. (a) Waveform for first higher order wave at $f = 290$ Hz and $\kappa = 0.2\ \mathrm{m}^{-1}$. (b) Waveform for second higher order wave at $f = 320$ Hz and $\kappa = 0.2\ \mathrm{m}^{-1}$.

3.2. Wind tunnel assessment

Fig. 15 shows the measured tunnel and plate acceleration for a flow speed of 120 m/s. The plate vibration has a maximum around the aerodynamic coincidence, predicted at 560 Hz [26]. The tunnel has a visible maximum at 300 Hz and at higher frequencies its vibrations approach the plate vibrations. Analysis shows that the difference in acceleration level between plate and tunnel is too low, compared to the requirements defined by the values in Fig. 14.

To reduce the tunnel vibrations and hence the vibration transmission to the plate, most of the tunnel was covered with a constrained layer damping treatment. This improved the velocity level difference at higher frequencies but not so much around 300 Hz.

The waveguide-FE calculation shows that there are two additional waves cut-on around 300 Hz, which increase the tunnel's modal density and, hence, its mobility. This may explain the increase in the tunnel vibrations above 300 Hz. Fig. 13 indicates that these waves have a

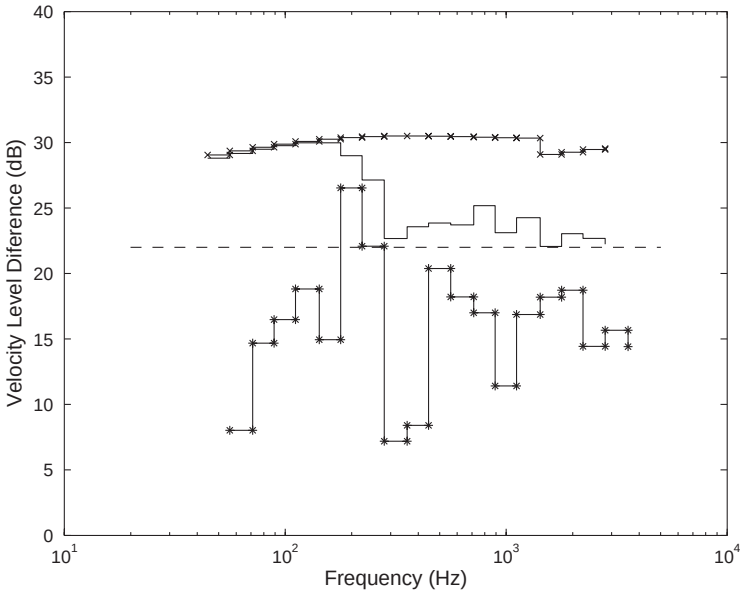

Fig. 14. Vibration velocity level difference between tunnel and plate when only the tunnel is externally excited. Conservative SEA estimates when the calculation of tunnel modal density is based on: — × —, Timoshenko beam theory; - - -, plate theory; —, waveguide FE. — ∗ —, measured data when tunnel is excited with a shaker.

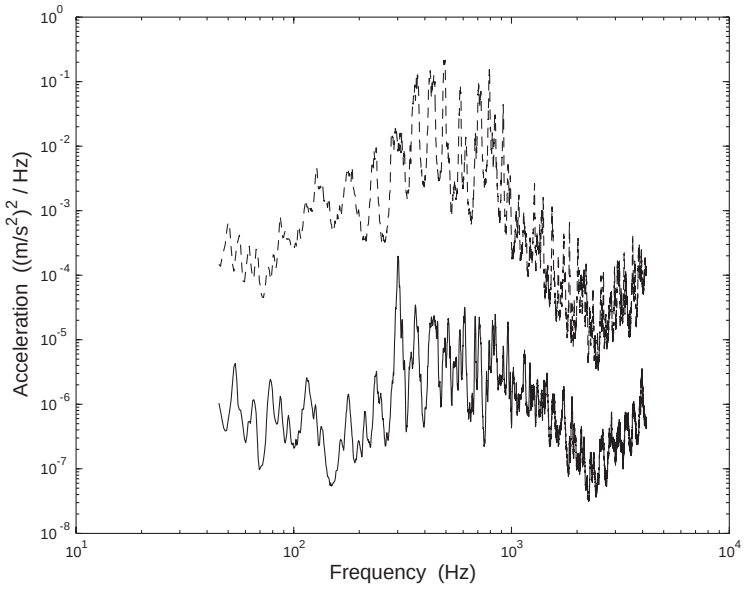

Fig. 15. Accelerations with 120 m/s flow speed in original wind tunnel. —, tunnel; - - -, test plate.

plate-character, involving flexural motion of the tunnel wall. Based on this evidence, two steel bars with a cross-section of 40×40 mm^2 were fitted on the tunnel's top face just in front and after the test plate. These bars have a considerable bending stiffness compared to that of the tunnel wall

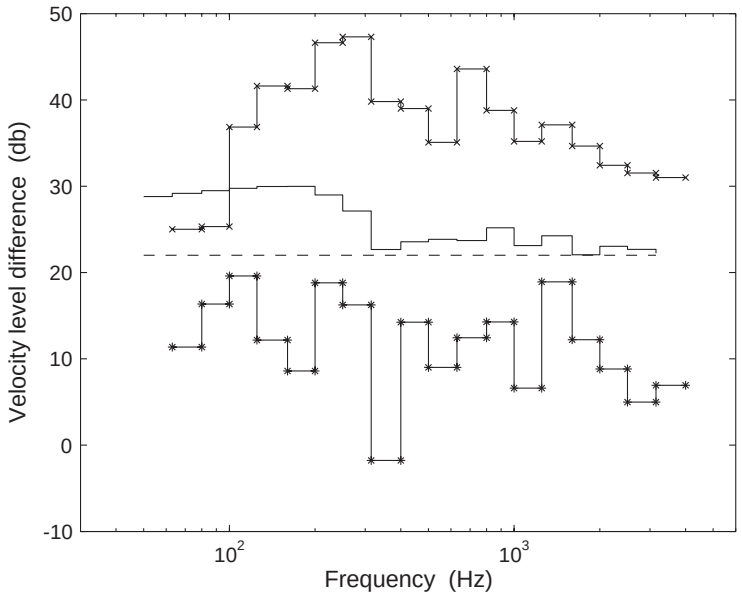

Fig. 16. Velocity level difference between test plate and wind tunnel for modified wind tunnel. — × —, measured with 120 m/s flow; ——, conservative SEA estimate for when tunnel only is excited; - - - -, 22 dB; — ∗ —, measured when tunnel is excited with a shaker.

and were designed to block the flexural vibration transmission. The effectiveness of these treatments is appreciated in Fig. 16, showing that the test plate vibrations above 100 Hz are induced by the turbulent flow and not by the tunnel vibrations.

4. Conclusions

The waveguide finite element method formulates a system of wave equations for complicated structures. From the wave equations follow dispersion relations, relating wavenumbers with frequency for propagating waves. These relations can be transformed into a linear eigenvalue problem and solved by efficient standard routines. The proven versatility of the FEM and the examples in the Refs. [6–17] suggest that the method may apply for any conceivable structure with cross-sectional properties that are uniform along one direction.

A critical input datum to a statistical energy analysis is the modal density. The calculation of SEA coupling loss factors using wave approach methodology, see, e.g., [2,3,24], requires the group velocity for the studied waves. The present work demonstrates, for the first time, the evaluation of these quantities based on the waveguide-FEM. The presentation is made via two examples.

The first example considers a channel beam with dimensions such that beam theories apply only in a lower-frequency regime. For this beam, the dispersion relations are solved and the results are compared with those from the Euler and Vlasov beam theories, showing that the Vlasov theory describes the wave motion at frequencies below 200 Hz, whereas the Euler beam theory cannot.

To the best of the author's knowledge, commercial SEA packages consider Euler and Timoshenko beam theories only. Therefore, these packages cannot be used for an SEA of the channel beam, except for higher frequencies for which the beam is likened to a plate assembly.

Higher order beam theory is complicated and requires cross-sectional data, which for complex sections may be difficult, if not impossible, to find in the literature. In contrast to this, the only data required for the waveguide-FEA are the geometry and the material data. Thus, even when beam theory applies, the waveguide-FEM seems advantageous, especially so, as calculations are readily made.

The second example considers a wind tunnel having an aluminium plate mounted into an aperture in its wall. A high-speed internal flow generates a turbulent fluctuating wall pressure, which excites vibrations in both the tunnel and the test plate. For studies of the test plate vibration, it is critical that the vibration transmission from the tunnel to the plate is small.

To estimate the vibration transmission from the tunnel to the plate, an SEA model is made and for this the modal densities of the tunnel and the plate are required. The plate's modal density is estimated by the expression for a thin-walled plate, taken from the literature. The tunnel is a more complicated structure, which behaves as a beam at low frequencies and as a plate assembly at high frequencies. To find the limits for these frequency regions and to study the intermediate frequency region, a waveguide-FE model of the tunnel was made. This model determines the characteristics of the vibrational waves in the tunnel and it facilitates the calculation of the modal density.

From the SEA it follows that the energy per mode in the plate cannot, on average, be higher than that of the tunnel, when the tunnel only is excited. Thus, if under operation the plate's modal energy is much higher than the tunnel's modal energy, it follows that the vibration transmission from tunnel to plate is insignificant compared to the direct TBL excitation. This gives a conservative estimate of the tunnel vibration's contribution to the test plate vibration by which the performance of the experimental setup can be assessed.

The presented calculation shows SEA at its best. For the considered range of frequencies, it would be hard, indeed, to calculate the response to turbulent excitation of the wind tunnel using standard methods. SEA, on the other hand, immediately provides a conservative estimate of the vibration transmission from the tunnel to the plate. The success of this simple SEA calculation is based on the presented procedure for the evaluation of the wind tunnel's modal density. Moreover, the extra information gained from the waveguide-FE analysis helped in devising measures to stop the vibration transmission from the wind tunnel to the test plate.

Acknowledgements

It is a pleasure to acknowledge the help from friends and colleagues: Dr. Urmas Ross for Fig. 10 and the wind tunnel measurements, Professor Ilkka Karasalo for the trick used in the derivation of equation (18), Carl-Magnus Nilsson for stimulating discussions and Dr. Andrew Peplow for reading the manuscript and suggesting improvements. The work was supported by the Swedish Research Council (260-2000-424 and 260-99-404) and the European Commission: ENABLE (GRD4_CT-00-00223).

Appendix A. Waveguide FE formulation

A.1. Strain energy for plate strip

Consider one of the strip elements that describe the channel beam in Fig. 1 or the wind tunnel in Fig. 10. The plate strip is in a local x–z plane with the local y-axis normal to the strip. The local z-axis coincides with the global z-axis and is in the direction of wave propagation.

For harmonic time dependence the strain energy for an orthotropic plate strip of thickness T_p, width $2l$ and in-definite length is given by

$$E_p = \int \mathrm{d}z \int_{-l}^{l} (e_{ip} + e_{bp})\,\mathrm{d}x = \int \mathrm{d}z \int_{-l}^{l} [\boldsymbol{\varepsilon}^*]^{\mathrm{T}} \mathbf{D} [\boldsymbol{\varepsilon}] + \frac{T_p^2}{12} [\boldsymbol{\chi}^*]^{\mathrm{T}} \mathbf{D} [\boldsymbol{\chi}]\,\mathrm{d}x, \tag{A.1}$$

where upper index * denotes complex conjugate, e_{ip} is the in-plane strain energy density, e_{bp} is the flexural strain energy density and

$$[\boldsymbol{\varepsilon}] = \left[\frac{\partial u}{\partial x} \quad \frac{\partial w}{\partial z} \quad \frac{\partial u}{\partial z} + \frac{\partial w}{\partial x}\right]^{\mathrm{T}}, \quad [\boldsymbol{\chi}] = \left[\frac{\partial^2 v}{\partial x^2} \quad \frac{\partial^2 v}{\partial z^2} \quad \frac{2\partial^2 v}{\partial x\ \partial z}\right]^{\mathrm{T}} \tag{A.2}$$

$$\mathbf{D} = \begin{bmatrix} B_x & B_{xz} & 0 \\ B_{xz} & B_z & 0 \\ 0 & 0 & G \end{bmatrix}. \tag{A.3}$$

u, v and w are the displacements, as functions of frequency, in the local x, y and z direction, respectively. For an isotropic plate,

$$B_x = B_z = \frac{T_p E}{(1-\nu^2)}, \quad B_{xz} = \nu B_x, \quad G = \frac{T_p E}{2(1+\nu)}, \tag{A.4}$$

where E is Young's modulus and ν is the Poisson ratio.

The expressions for the strain energy densities are expanded, resulting in

$$\begin{aligned} e_{ip} = {} & B_x \frac{\partial u^*}{\partial x}\frac{\partial u}{\partial x} + B_{xz}\frac{\partial u^*}{\partial x}\frac{\partial w}{\partial z} + B_{xz}\frac{\partial w^*}{\partial z}\frac{\partial u}{\partial x} + B_z \frac{\partial w^*}{\partial z}\frac{\partial w}{\partial z} \\ & + G\left[\frac{\partial u^*}{\partial z}\frac{\partial u}{\partial z} + \frac{\partial u^*}{\partial z}\frac{\partial w}{\partial x} + \frac{\partial w^*}{\partial x}\frac{\partial u}{\partial z} + \frac{\partial w^*}{\partial x}\frac{\partial w}{\partial x}\right], \end{aligned} \tag{A.5}$$

$$\begin{aligned} e_{bp} = {} & \frac{T_p^2}{12}\left[B_x \frac{\partial^2 v^*}{\partial x^2}\frac{\partial^2 v}{\partial x^2} + B_{xz}\frac{\partial^2 v^*}{\partial x^2}\frac{\partial^2 v}{\partial z^2} + B_{xz}\frac{\partial^2 v^*}{\partial z^2}\frac{\partial^2 v}{\partial x^2}\right. \\ & \left. + B_z \frac{\partial^2 v^*}{\partial z^2}\frac{\partial^2 v}{\partial z^2} + 4G\frac{\partial^2 v^*}{\partial x\ \partial z}\frac{\partial^2 v}{\partial x\ \partial z}\right]. \end{aligned} \tag{A.6}$$

A.2. Shape functions

Polynomial shape functions that describe the motion's x-dependence are assumed in the form of

$$u(x,z) = \mathbf{f}(\xi) * \mathbf{B_u} * \mathbf{V}(z); \quad v(x,z) = \mathbf{g}(\xi) * \mathbf{B_v} * \mathbf{V}(z), \quad w(x,z) = \mathbf{f}(\xi) * \mathbf{B_w} * \mathbf{V}(z), \tag{A.7}$$

where the entries of the vector $\mathbf{V}$ are the three displacement components and the rotation about the z-axis along the lines $x = \pm l$, plus any additional internal degrees of freedom and

$$\mathbf{f}(\xi) = [1 \quad \xi \quad \ldots \quad \xi^n], \quad \mathbf{g}(\xi) = [1 \quad \xi \quad \ldots \quad \xi^m], \quad \xi = x/l. \tag{A.8}$$

Implemented in the routine used in the calculations is that the in-plane vibrations u and w are described by linear FE shapefunctions whereas the out of plane vibrations are described by cubic polynomials. Thus, in Eq. (A.8) $n = 1$ and $m = 3$. The eight variational parameters in $\mathbf{V}$ are then the three displacement components plus the rotation about the z-axis at the two nodes. This choice of parameters and the definitions of $\mathbf{f}$ and $\mathbf{g}$ determine the matrices $\mathbf{B_u}, \mathbf{B_v}$ and $\mathbf{B_w}$.

A.3. Evaluation of the stiffness matrix

The shape functions defined by Eq. (A.7) are inserted into the expression for strain energy (A.1) and the integrals and derivatives with respect to x are evaluated, resulting in

$$\int e_{ip}\,\mathrm{d}x = [\mathbf{V}^*]^{\mathrm{T}}\mathbf{A_{00}}\mathbf{V} + \left[\frac{\partial \mathbf{V}^a}{\partial z}\right]^{\mathrm{T}}\mathbf{A_{10}}\mathbf{V} + [\mathbf{V}^*]^{\mathrm{T}}\mathbf{A_{01}}\left[\frac{\partial \mathbf{V}}{\partial z}\right] + \left[\frac{\partial \mathbf{V}^*}{\partial z}\right]^{\mathrm{T}}[\mathbf{A_{11}}]\left[\frac{\partial \mathbf{V}}{\partial z}\right], \tag{A.9}$$

$$\int e_{bp}\,\mathrm{d}x = [\mathbf{V}^*]^{\mathrm{T}}\mathbf{B_{00}}\mathbf{V} + \left[\frac{\partial \mathbf{V}^*}{\partial z}\right]^{\mathrm{T}}[\mathbf{B_{11}}]\left[\frac{\partial \mathbf{V}}{\partial z}\right] + \left[\frac{\partial^2 \mathbf{V}^*}{\partial z^2}\right]^{\mathrm{T}}\mathbf{B_{20}}\mathbf{V} + [\mathbf{V}^*]^{\mathrm{T}}\mathbf{B_{02}}\left[\frac{\partial^2 \mathbf{V}}{\partial z^2}\right] + \left[\frac{\partial^2 \mathbf{V}^*}{\partial z^2}\right]^{\mathrm{T}}[\mathbf{B_{22}}]\left[\frac{\partial^2 \mathbf{V}}{\partial z^2}\right], \tag{A.10}$$

where

$$\mathbf{A_{nm}} = \mathbf{A_{mn}^{\mathrm{T}}}, \quad \mathbf{B_{nm}} = \mathbf{B_{mn}^{\mathrm{T}}}. \tag{A.11}$$

$$\begin{aligned}
\mathbf{A_{00}} &= B_x\mathbf{B_u^{\mathrm{T}}}\mathbf{I_{1.1}}\mathbf{B_u} + G\mathbf{B_w^{\mathrm{T}}}\mathbf{I_{1.1}}\mathbf{B_w},\\
\mathbf{A_{10}} &= B_{xz}\mathbf{B_w^{\mathrm{T}}}\mathbf{I_{0.1}}\mathbf{B_u} + G\mathbf{B_u^{\mathrm{T}}}\mathbf{I_{0.1}}\mathbf{B_w},\\
\mathbf{A_{11}} &= B_z\mathbf{B_w^{\mathrm{T}}}\mathbf{I_{0.0}}\mathbf{B_w} + G\mathbf{B_u^{\mathrm{T}}}\mathbf{I_{0.0}}\mathbf{B_u},
\end{aligned} \tag{A.12}$$

$$\mathbf{B_{00}} = \frac{B_x T_p^2}{12}[\mathbf{B_v}]^{\mathrm{T}}\mathbf{J_{2.2}}\mathbf{B_v}, \quad \mathbf{B_{11}} = \frac{GT_p^2}{12}[\mathbf{B_v}]^{\mathrm{T}}\mathbf{J_{1.1}}\mathbf{B_v},$$

$$\mathbf{B_{02}} = \frac{B_{xz} T_p^2}{12}[\mathbf{B_v}]^{\mathrm{T}}\mathbf{J_{0.2}}\mathbf{B_v}, \quad \mathbf{B_{22}} = \frac{B_z T_p^2}{12}[\mathbf{B_v}]^{\mathrm{T}}\mathbf{J_{0.0}}\mathbf{B_v}, \tag{A.13}$$

$$\mathbf{I_{n.m}} = \int_{-l}^{l}\left[\frac{\partial^n \mathbf{f}}{\partial \mathbf{x}^n}\right]^{\mathrm{T}} * \left[\frac{\partial^m \mathbf{f}}{\partial \mathbf{x}^m}\right]\mathrm{d}x, \quad \mathbf{J_{n.m}} = \int_{-l}^{l}\left[\frac{\partial^n \mathbf{g}}{\partial \mathbf{x}^n}\right]^{\mathrm{T}} * \left[\frac{\partial^m \mathbf{g}}{\partial \mathbf{x}^m}\right]\mathrm{d}x. \tag{A.14}$$

The integrals and derivatives in Eq. (A.14) are conveniently, and exactly, evaluated with the routines "Dif" and "Int" in Ref. [15, Section 3.1] or by explicit derivation and Gaussian integration, e.g. Ref. [27].

A.4. Equations of motion

The 'Lagrangian' describing free motion of the plate is given by

$$L_p = E_p - E_k, \tag{A.15}$$

where E_p is the strain energy, given by Eqs. (A.1), (A.9) and (A.10) while E_k is the kinetic energy, which is given by

$$E_k = \int \mathrm{d}z \int_{-l}^{l} \omega^2 \rho T_p (u^* u + v^* v + w^* w)\,\mathrm{d}x = \omega^2 \int [\mathbf{V}^*]^{\mathrm{T}} \mathbf{M} [\mathbf{V}]\,\mathrm{d}z, \tag{A.16}$$

$$\mathbf{M} = \rho T_p (\mathbf{B}_\mathbf{u}^{\mathrm{T}} \mathbf{I}_{0.0} \mathbf{B}_\mathbf{u} + \mathbf{B}_\mathbf{v}^{\mathrm{T}} \mathbf{J}_{0.0} \mathbf{B}_\mathbf{v} + \mathbf{B}_\mathbf{w}^{\mathrm{T}} \mathbf{I}_{0.0} \mathbf{B}_\mathbf{w}). \tag{A.17}$$

The corresponding set of Euler–Lagrange equations is [28, Chapter 3]

$$\mathbf{K_4} \frac{\partial^4 \mathbf{V}}{\partial z^4} + \mathbf{K_3} \frac{\partial^3 \mathbf{V}}{\partial z^3} + \mathbf{K_2} \frac{\partial^2 \mathbf{V}}{\partial z^2} + \mathbf{K_1} \frac{\partial \mathbf{V}}{\partial z} + \mathbf{K_0} \mathbf{V} - \omega^2 \mathbf{M} \mathbf{V} = \mathbf{0}, \tag{A.18}$$

where

$$\begin{aligned} &\mathbf{K_4} = \mathbf{B_{22}}, \quad \mathbf{K_3} = \mathbf{0}, \quad \mathbf{K_2} = \mathbf{B_{20}} + \mathbf{B_{02}} - \mathbf{B_{11}} - \mathbf{A_{11}}, \\ &\mathbf{K_1} = \mathbf{A_{01}} - \mathbf{A_{10}}, \quad \mathbf{K_0} = \mathbf{B_{00}} + \mathbf{A_{00}}. \end{aligned} \tag{A.19}$$

The matrices $\mathbf{K_n}$ and $\mathbf{M}$ are calculated for each element and the matrices are assembled using standard FE procedures [27], thus producing Eq. (1).

References

[1] L. Cremer, M. Heckl, E.E. Ungar, *Structure-borne Sound*, Springer, Berlin, 1988.
[2] R.H. Lyon, R.G. DeJong, *Theory and Application of SEA*, Butterworth, London, 1995.
[3] R.J.M. Craik, *Sound Transmission Through Buildings using Statistical Energy Analysis*, Gower press, London, 1996.
[4] R.S. Langley, The modal density and mode count of thin cylinders and curved panels, *Journal of Sound and Vibration* 169 (1994) 43–53.
[5] S. Finnveden, Formulas for modal density and for input power from mechanical and fluid point sources in fluid filled pipes, *Journal of Sound and Vibration* 208 (1997) 705–728.
[6] B. Aalami, Waves in prismatic guides of arbitrary cross section, *Journal of Applied Mechanics* 40 (1973) 1067–1072.
[7] S.K. Datta, A.H. Shah, R.L. Bratton, T. Chakraborty, Wave propagation in laminated composite plates, *Journal of the Acoustical Society of America* 83 (1988) 2020–2026.
[8] L. Gavric, Finite element computation of dispersion properties of thin-walled waveguides, *Journal of Sound and Vibration* 173 (1994) 113–124.
[9] L. Gavric, Computation of propagative waves in free rail using a finite element technique, *Journal of Sound and Vibration* 184 (1995) 531–543.
[10] L. Gry, Dynamic modelling of railway track based on wave-propagation, *Journal of Sound and Vibration* 195 (1997) 477–505.
[11] U. Orrenius, S. Finnveden, Calculation of wave propagation in rib-stiffened plate structures, *Journal of Sound and Vibration* 198 (1996) 203–224.
[12] O. Onipede, S.B. Dong, Propagating waves and end modes in pretwisted beams, *Journal of Sound and Vibration* 195 (1996) 313–330.
[13] T. Mazuch, Wave dispersion in anisotropic shells and rods by the finite element method, *Journal of Sound and Vibration* 198 (1996) 429–438.

[14] V.V. Volovoi, D.H. Hodges, V.L. Berdichevsky, V.G. Sutyrin, Dynamic dispersion curves for non-homogenous, anisotropic beams with cross-section of arbitrary geometry, *Journal of Sound and Vibration* 215 (1998) 1101–1120.
[15] S. Finnveden, Spectral finite element analysis of the vibration of straight fluid-filled pipes with flanges, *Journal of Sound and Vibration* 199 (1997) 125–154.
[16] C-M. Nilsson, S. Finnveden, Input of vibration energy into waveguides using FE-formulations, *Proceedings NOVEM-2000*, *Lyon*, 2000.
[17] C-M. Nilsson, Waveguide Finite Elements for Thin-Walled Structures, Licentiate Thesis, KTH, TRITA_FKT 2002:02, 2002.
[18] G. Strang, *Introduction to Applied Mathematics*, Wellesly-Cambridge Press, Wellesly, MA, 1986.
[19] F. Tisseur, K. Meerbergen, The quadratic eigenvalue problem, *SIAM Review* 43 (2001) 235–286.
[20] J.T. Oden, *Mechanics of Elastic Structures*, McGraw-Hill, New York, 1967.
[21] P.O. Friberg, Beam element matrices derived from Vlasov's theory of open thin-walled elastic beams, *International Journal of Numerical Methods in Engineering* 21 (1985) 1205–1228.
[22] L.P. Kollar, Flexural–torsional vibration of open section composite beams with shear deformation, *Journal of Solids and Structures* 38 (2001) 7543–7558.
[23] R.S. Langley, A wave intensity technique for the analysis of high frequency vibrations, *Journal of Sound and Vibration* 159 (1992) 483–502.
[24] R.S. Langley, K.H. Heron, Elastic wave transmission through plate/beam junctions, *Journal of Sound and Vibration* 143 (1990) 241–253.
[25] A. Bocquillet, M.N. Ichchou, L. Jezequel, Energetics of fluid filled pipes up to high frequencies, *Journal of Fluids and Structures* 17 (2003) 491–510.
[26] G. Cousin, Sound from TBL Induced Vibrations, Licentiate Thesis, KTH, TRITA_FKT 1999:35, 1999.
[27] O.C. Zienkiewicz, *The Finite Element Method*, McGraw-Hill, New York, 1997.
[28] P.M. Morse, H. Feshbach, *Methods of Theoretical Physics*, McGraw-Hill, New York, 1953.